

# Charmonium dynamics in nucleus-nucleus collisions at SPS and FAIR energies

O. Linnyk,<sup>a,\*</sup> E. L. Bratkovskaya,<sup>a</sup> W. Cassing,<sup>c</sup> H. Stöcker<sup>a,b</sup>

<sup>a</sup> *Frankfurt Institute for Advanced Studies, Johann Wolfgang Goethe University, Max-von-Laue-Str. 1, 60438 Frankfurt am Main, Germany*

<sup>b</sup> *Institut für Theoretische Physik, Johann Wolfgang Goethe University, Max-von-Laue-Str. 1, 60438 Frankfurt am Main, Germany*

<sup>c</sup> *Institut für Theoretische Physik, Universität Giessen, D-35392 Giessen, Germany*

---

## Abstract

Charmonium production and suppression in In+In and Pb+Pb reactions at SPS energies is investigated with the HSD transport approach within the ‘hadronic comover model’ as well as the ‘QGP threshold scenario’. The results of the transport calculations for  $J/\Psi$  suppression and the  $\Psi'$  to  $J/\Psi$  ratio are compared with the recent data of the NA50 and NA60 Collaborations. We find that the comover absorption model – with a single parameter  $|M_0|^2$  for the matrix element squared for charmonium-meson dissociation – performs best with respect to all data sets. The ‘threshold scenario’ – within different assumptions for the melting energy densities – yields a reasonable suppression for  $J/\Psi$  but fails in reproducing the  $\Psi'$  to  $J/\Psi$  ratio for Pb+Pb at 158 A·GeV. Predictions for Au+Au reactions are presented for a bombarding energy of 25 A·GeV in the different scenarios which will allow for a clear distinction between the models from the experimental side at the future FAIR facility.

*Key words:* Relativistic heavy-ion collisions, Meson production, Quark-gluon plasma, Charmed mesons, Charmed quarks

PACS 25.75.-q, 13.60.Le, 12.38.Mh, 14.40.Lb, 14.65.Dw

---

\* corresponding author

*Email address:* linnyk@fias.uni-frankfurt.de (O. Linnyk,).

## 1 Introduction

The dynamics of ultra-relativistic nucleus-nucleus collisions at Super-Proton-Synchrotron (SPS) and Relativistic-Heavy-Ion-Collider (RHIC) energies are of fundamental interest with respect to the properties of hadronic/partonic systems at high energy densities. Especially the formation of a quark-gluon plasma (QGP) and its transition to interacting hadronic matter has motivated a large community for almost three decades [1]. The  $c, \bar{c}$  quark degrees of freedom are of particular interest in context to the phase transition to the QGP, since  $c\bar{c}$  meson states might no longer be formed due to color screening [2,3,4,5]. However, more recent lattice QCD (lQCD) calculations have shown that the  $J/\Psi$  survives up to at least  $1.5 T_c$  ( $T_c \approx 170$  MeV) such that the lowest  $c\bar{c}$  states remain bound up to rather high energy density [6,7,8]. On the other hand the  $\chi_c$  and  $\Psi'$  appear to melt soon above  $T_c$ . It is presently not clear if also the  $D$  or  $D^*$  mesons will survive at temperatures  $T > T_c$  but strong correlations between a light quark (antiquark) and a charm antiquark (quark) are likely to persist [9].

The standard approach to charmonium production in heavy-ion collisions assumes that  $c\bar{c}$  pairs are created exclusively at the initial stage of the reaction in primary nucleon-nucleon collisions. At the very early stage color dipole states are expected to be formed which experience i) absorption by interactions with nucleons of the colliding nuclei (*cf.* Refs. [10,11]). These  $c\bar{c}$  states are assumed to be absorbed in a ‘pre-resonance state’ before the final hidden charm mesons are formed. This absorption – denoted by ‘normal nuclear suppression’ – is also present in p+A reactions and determined by a dissociation cross section  $\sigma_B \sim 4$  to 7 mb). Those charmonia or ‘pre-resonance’ states – that survive normal nuclear suppression – furthermore suffer from ii) a possible dissociation in the deconfined medium at sufficiently high energy density and iii) the interactions with secondary hadrons (comovers) formed in a later stage of the nucleus-nucleus collision.

The geometrical Glauber model of Blaizot et al. [12], as well as the percolation model of Satz [4], assumes that the QGP suppression ii) sets in rather abruptly as soon as the energy density exceeds a threshold value  $\varepsilon_c$ , which is a free parameter. This version of the standard approach will be referred to as the QGP ‘threshold scenario’. The latter model is motivated by the idea that the charmonium dissociation rate is drastically larger in a quark-gluon-plasma (QGP) than in a hadronic medium [4] such that further comover absorption channels might be neglected.

On the other hand, the extra suppression of charmonia in the high density phase of nucleus-nucleus collisions at SPS energies [13,14,15,16,17,18] has been attributed to inelastic comover scattering (*cf.* [11,19,20,21,22,23,24,25]) and

Refs. therein) assuming that the corresponding  $J/\Psi$ -hadron cross sections are in the order of a few mb [26,27,28,29]. Theoretical estimates here differ by more than an order of magnitude [30] especially with respect to  $J/\Psi$ -meson scattering such that the question of charmonium suppression is still open. Additionally, alternative absorption mechanisms – such as gluon scattering on color dipole states – might play a role as suggested in Refs. [31,32,33,34] and also lead to a reduction of the final  $J/\Psi$  formation in central nucleus-nucleus collisions.

We recall that apart from absorption or dissociation channels for charmonia also recombination channels such  $D + \bar{D} \rightarrow J/\Psi + \text{meson}$  may play a role. A previous analysis within the HSD transport approach [35] – employing the comover absorption model – has demonstrated that the charmonium production from open charm and anticharm mesons indeed becomes essential in central Au+Au collisions at RHIC. This is in accordance with independent studies in Refs. [28,32] and also with the data from PHENIX [36]. On the other hand, these backward channels – relative to charmonium dissociation with comoving mesons – have been found to be practically negligible at the SPS energies of interest here. Nevertheless, in our dynamical studies below we will include the ‘backward’ channels for completeness.

A couple of models have predicted  $J/\Psi$  suppression in In+In collisions as a function of centrality at 158 A·GeV based on the parameters fixed for Pb+Pb reactions at the same bombarding energy. However, the predictions within the comover model and ‘threshold scenario’ from Refs. [38,37,39] have failed to describe the data with sufficient accuracy. This might be either due to the missing dynamics of the nucleus-nucleus collisions in these models or to inadequate physical assumptions about the dissociation mechanism.

In the present work we extend the previous studies within the comover model in Refs. [40,35,41] and test the ‘QGP threshold scenario’ – described in Section 2 – in comparison to the Pb+Pb data at 158 A·GeV from NA50 as well the high statistics data from NA60 for In+In collisions at the same bombarding energy. The question we aim at solving in Section 3 is: 1) can any of the models be ruled out by the combined data sets and 2) do the recent NA60 data provide a hint to QGP formation at the top SPS energy? In Section 4 we, furthermore, will provide predictions for the charmonium suppression in Au+Au collisions at 25 A·GeV that will be measured at the future FAIR facility by the CBM Collaboration.

## 2 Brief description of charmonium channels in HSD

The microscopic Hadron-String-Dynamics (HSD) transport calculations (employed here) provide the space-time geometry of the nucleus-nucleus reaction and a rather reliable estimate for the local energy densities achieved since the production of secondary particles is described rather well from SIS to RHIC energies [42]. In order to examine the dynamics of open charm and charmonium degrees of freedom during the formation and expansion phase of the highly excited system created in a relativistic nucleus-nucleus collision within transport approaches, one has to know the number of initially produced particles with  $c$  or  $\bar{c}$  quarks, i.e.  $D, \bar{D}, D^*, \bar{D}^*, D_s, \bar{D}_s, D_s^*, \bar{D}_s^*, J/\Psi(1S), \Psi'(2S), \chi_c(1P)$ . In this work we follow the previous studies in Refs. [19,22,35,40] and fit the total charmonium cross sections ( $i = \chi_c, J/\Psi, \Psi'$ ) from  $NN$  collisions as a function of the invariant energy  $\sqrt{s}$  by the expression

$$\sigma_i^{NN}(s) = f_i a \left(1 - \frac{m_i}{\sqrt{s}}\right)^\alpha \left(\frac{\sqrt{s}}{m_i}\right)^\beta \theta(\sqrt{s} - \sqrt{s_{0i}}), \quad (1)$$

where  $m_i$  denotes the mass of charmonium  $i$  while  $\sqrt{s_{0i}} = m_i + 2m_N$  is the threshold in vacuum. The parameters in (1) have been fixed to describe the  $J/\Psi$  and  $\Psi'$  data up to the RHIC energy  $\sqrt{s} = 200$  GeV (*cf.* Fig. 1). We use  $a = 0.2$  mb,  $\alpha = 10$ ,  $\beta = 0.775$ . The parameters  $f_i$  are fixed as  $f_{\chi_c} = 0.636$ ,  $f_{J/\Psi} = 0.581$ ,  $f_{\Psi'} = 0.21$  in order to reproduce the experimental ratio

$$\frac{B(\chi_{c1} \rightarrow J/\Psi)\sigma_{\chi_{c1}} + B(\chi_{c2} \rightarrow J/\Psi)\sigma_{\chi_{c2}}}{\sigma_{J/\Psi}^{exp}} = 0.344 \pm 0.031$$

measured in  $pp$  and  $\pi N$  reactions [43,44] as well as the averaged  $pp$  and  $pA$  ratio  $(B_{\mu\mu}(\Psi')\sigma_{\Psi'})/(B_{\mu\mu}(J/\Psi)\sigma_{J/\Psi}) \simeq 0.0165$  (*cf.* the compilation of experimental data in Ref. [45]). Here the experimentally measured  $J/\Psi$  cross section includes the direct  $J/\Psi$  component ( $\sigma_{J/\Psi}$ ) as well as the decays of higher charmonium states  $\chi_c, \Psi'$ , *i.e.*

$$\sigma_{J/\Psi}^{exp} = \sigma_{J/\Psi} + B(\chi_c \rightarrow J/\Psi)\sigma_{\chi_c} + B(\Psi' \rightarrow J/\Psi)\sigma_{\Psi'}. \quad (2)$$

Note, we do not distinguish the  $\chi_{c1}(1P)$  and  $\chi_{c2}(1P)$  states. Instead, we use only the  $\chi_{c1}(1P)$  state (which we denote as  $\chi_c$ ), however, with an increased branching ratio for the decay to  $J/\Psi$  in order to include the contribution of  $\chi_{c2}(1P)$ , *i.e.*  $B(\chi_c \rightarrow J/\Psi) = 0.54$ . We adopt  $B(\Psi' \rightarrow J/\Psi) = 0.557$  from Ref. [46].

In addition to primary hard  $NN$  collisions the open charm mesons or charmonia may also be generated by secondary meson-baryon ( $mB$ ) reactions. Here

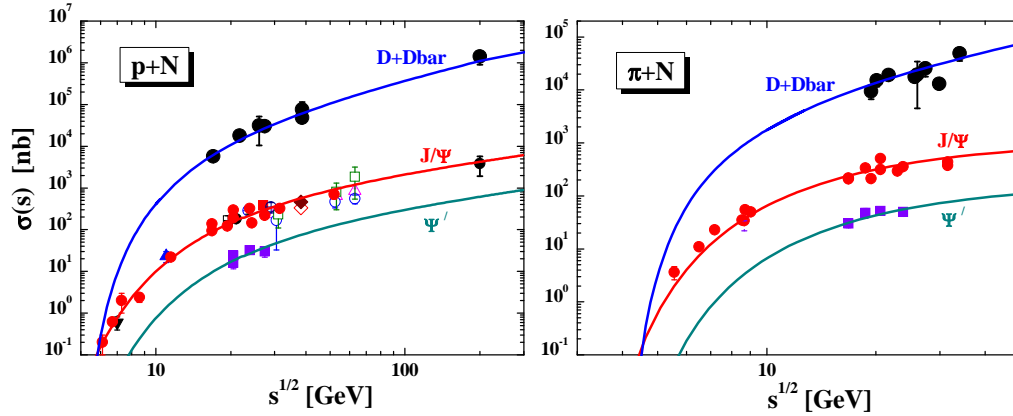


Fig. 1. The cross section for  $D + \bar{D}$ ,  $J/\Psi$  and  $\Psi'$  meson production in  $pN$  (left part) and  $\pi N$  reactions (right part). The solid lines show the parametrizations used in HSD, whereas the symbols stand for the experimental data [48,49,50,51,52,53,54,55,56,57]. The  $J/\Psi$  cross sections include the decay from  $\chi_c$  mesons.

we include all secondary collisions of mesons with baryons by assuming that the open charm cross section (from Section 2 of Ref. [40]) only depends on the invariant energy  $\sqrt{s}$  and not on the explicit meson or baryon state. Furthermore, we take into account all interactions of ‘formed’ mesons – after a formation time of  $\tau_F = 0.8$  fm/c (in their rest frame) [47] – with baryons or diquarks, respectively. For the total charmonium cross sections from meson-baryon (or  $\pi N$ ) reactions we use the parametrization (in line with Ref. [20]):

$$\sigma_i^{\pi N}(s) = f_i b \left(1 - \frac{m_i}{\sqrt{s}}\right)^\gamma \quad (3)$$

with  $\gamma = 7.3$  and  $b = 1.24$  mb, which describes the existing experimental data at low  $\sqrt{s}$  reasonably well as seen from Fig. 1.

Apart from the total cross sections, we also need the differential distribution of the produced mesons in the transverse momentum  $p_T$  and the rapidity  $y$  (or Feynman  $x_F$ ) from each individual collision. We recall that  $x_F = p_z/p_z^{max} \approx 2p_z/\sqrt{s}$  with  $p_z$  denoting the longitudinal momentum. For the differential distribution in  $x_F$  from  $NN$  and  $\pi N$  collisions we use the ansatz from the E672/E706 Collaboration [58]:

$$\frac{dN}{dx_F dp_T} \sim (1 - |x_F|)^c \exp(-b_{p_T} p_T), \quad (4)$$

where  $b_{p_T} = 2.08$  GeV $^{-1}$  and  $c = a/(1+b/\sqrt{s})$ . The parameters  $a, b$  are chosen as  $a_{NN} = 13.5$ ,  $b_{NN} = 24.9$  for  $NN$  collisions and  $a_{\pi N} = 4.11$ ,  $b_{\pi N} = 10.2$  for  $\pi N$  collisions as in [35,40].

The parametrizations of the total and differential cross sections for open charm

mesons from  $pN$  and  $\pi N$  collisions are taken as in Refs. [35,40]. Here we show only the total cross sections for  $D + \bar{D}$  productions in Fig. 1.

In order to study the effect of charmonium rescattering we adopt the following dissociation cross sections of charmonia with baryons independent of the energy (in line with the recent NA50 and NA60 compilations [18,59]):

$$\begin{aligned} \sigma_{c\bar{c}B} &= 4.18 \text{ mb}; \\ \sigma_{J/\Psi B} &= 4.18 \text{ mb}; \quad \sigma_{\chi_{cB}} = 4.18 \text{ mb}; \quad \sigma_{\Psi' B} = 7.6 \text{ mb}. \end{aligned} \tag{5}$$

In (5) the cross section  $\sigma_{c\bar{c}B}$  stands for a (color dipole) pre-resonance ( $c\bar{c}$ ) - baryon cross section, since the  $c\bar{c}$  pair produced initially cannot be identified with a particular hadron due to the uncertainty relation in energy and time. For the life-time of the pre-resonance  $c\bar{c}$  pair (in its rest frame) a value of  $\tau_{c\bar{c}} = 0.3 \text{ fm}/c$  is assumed following Ref. [60]. This value corresponds to the mass difference of the  $\Psi'$  and  $J/\Psi$ .

For  $D, D^*, \bar{D}, \bar{D}^*$  - meson ( $\pi, \eta, \rho, \omega$ ) scattering we address to the calculations from Ref. [27,28] which predict elastic cross sections in the range of 10–20 mb depending on the size of the formfactor employed. As a guideline we use a constant cross section of 10 mb for elastic scattering with mesons and also baryons, although the latter might be even higher for very low relative momenta. Since the  $D$ -meson dynamics is of minor importance for charmonium regeneration at SPS energies we discard a more detailed description.

### 2.1 The comover absorption model

As already pointed out before, the  $J/\Psi, \chi_c, \Psi'$  formation cross sections by open charm mesons or the inverse comover dissociation cross sections are not well known and the significance of these channels is discussed controversially in the literature [30,62,63,64,65,66,67]. We here follow the concept of Refs. [35,41] and introduce a simple 2-body transition model with a single parameter  $|M_0|^2$ , that allows to implement the backward reactions uniquely by employing detailed balance for each individual channel.

Since the charmonium-meson dissociation and backward reactions typically occur with low relative momenta ('comovers') it is legitimate to write the cross section for the process  $1 + 2 \rightarrow 3 + 4$  as

$$\sigma_{1+2 \rightarrow 3+4}(s) = 2^4 \frac{E_1 E_2 E_3 E_4}{s} |\tilde{M}_i|^2 \left( \frac{m_3 + m_4}{\sqrt{s}} \right)^6 \frac{p_f}{p_i}, \tag{6}$$

where  $E_k$  denotes the energy of hadron  $k$  ( $k = 1, 2, 3, 4$ ), respectively. The

initial and final momenta for fixed invariant energy  $\sqrt{s}$  are given by

$$\begin{aligned} p_i^2 &= \frac{(s - (m_1 + m_2)^2)(s - (m_1 - m_2)^2)}{4s}, \\ p_f^2 &= \frac{(s - (m_3 + m_4)^2)(s - (m_3 - m_4)^2)}{4s}, \end{aligned} \quad (7)$$

where  $m_k$  denotes the mass of hadron  $k$ . In (6)  $|\tilde{M}_i|^2$  ( $i = \chi_c, J/\psi, \psi'$ ) stands for the effective matrix element squared, which for the different 2-body channels is taken of the form

$$\begin{aligned} |\tilde{M}_i|^2 &= |M_i|^2 \quad \text{for } (\pi, \rho) + (c\bar{c})_i \rightarrow D + \bar{D} \\ |\tilde{M}_i|^2 &= 3|M_i|^2 \quad \text{for } (\pi, \rho) + (c\bar{c})_i \rightarrow D^* + \bar{D}, D + \bar{D}^*, D^* + \bar{D}^* \\ |\tilde{M}_i|^2 &= \frac{1}{3}|M_i|^2 \quad \text{for } (K, K^*) + (c\bar{c})_i \rightarrow D_s + \bar{D}, \bar{D}_s + D \\ |\tilde{M}_i|^2 &= |M_i|^2 \quad \text{for } (K, K^*) + (c\bar{c})_i \rightarrow D_s + \bar{D}^*, \bar{D}_s + D^*, D_s^* + \bar{D}, \\ &\quad \bar{D}_s^* + D, \bar{D}_s^* + D^* \end{aligned} \quad (8)$$

The relative factors of 3 in (8) are guided by the sum rule studies in [68] which suggest that the cross section is increased whenever a vector meson  $D^*$  or  $\bar{D}^*$  appears in the final channel while another factor of 1/3 is introduced for each  $s$  or  $\bar{s}$  quark involved. The factor  $((m_3 + m_4)/\sqrt{s})^6$  in (6) accounts for the suppression of binary channels with increasing  $\sqrt{s}$  and has been fitted to the experimental data for the reactions  $\pi + N \rightarrow \rho + N, \omega + N, \phi + N, K^+ + \Lambda$  in Ref. [69].

We use (for simplicity) the same matrix elements for the dissociation of all charmonium states  $i$  ( $i = \chi_c, J/\psi, \psi'$ ) with mesons:

$$|M_{J/\Psi}|^2 = |M_{\chi_c}|^2 = |M_{\Psi'}|^2 = |M_0|^2. \quad (9)$$

We note that in Ref. [35] the parameter  $|M_0|^2$  was fixed by comparison to the  $J/\Psi$  suppression data from the NA38 and NA50 Collaborations for S+U and Pb+Pb collisions at 200 and 158 A·GeV, respectively. In the present study, however, this parameter has to be readjusted in accordance with the updated value of the cross section (5) of charmonium dissociation on baryons (following the latest NA50 and NA60 analysis [18,59]). The best fit is obtained for  $|M_0|^2 = 0.18 \text{ fm}^2/\text{GeV}^2$ .

The advantage of the model introduced in [35,41] is that detailed balance for the binary reactions can be employed strictly for each individual channel, *i.e.*

$$\sigma_{3+4 \rightarrow 1+2}(s) = \sigma_{1+2 \rightarrow 3+4}(s) \frac{(2S_1 + 1)(2S_2 + 1)}{(2S_3 + 1)(2S_4 + 1)} \frac{p_i^2}{p_f^2}, \quad (10)$$

and the role of the backward reactions ( $(c\bar{c})_i$ +meson formation by  $D + \bar{D}$  flavor exchange) can be explored without introducing any additional parameter once  $|M_i|^2$  is fixed. In Eq. (10) the quantities  $S_j$  denote the spins of the particles, while  $p_i^2$  and  $p_f^2$  denote the cms momentum squared in the initial and final channels, respectively. The uncertainty in the cross sections (10) is of the same order of magnitude as that in Lagrangian approaches using *e.g.*  $SU(4)_{flavor}$  symmetry [27,28], since the formfactors at the vertices are essentially unknown [68]. It should be pointed out that the comover dissociation channels for charmonia are described in HSD with the proper individual thresholds for each channel in contrast to the more schematic comover absorption model [11].

We recall that (as in Refs. [35,40,70,71,72]) the charm degrees of freedom in the HSD approach are treated perturbatively and that initial hard processes (such as  $c\bar{c}$  or Drell-Yan production from  $NN$  collisions) are ‘precalculated’ to achieve a scaling of the inclusive cross section with the number of projectile and target nucleons as  $A_P \times A_T$  when integrating over impact parameter. For fixed impact parameter  $b$  the  $c\bar{c}$  yield then scales with the number of binary hard collisions  $N_{bin}$  (*cf.* Fig. 8 in Ref. [40]).

## 2.2 Implementation of the ‘threshold scenario’

The HSD transport model allows to calculate the energy-momentum tensor  $T_{\mu\nu}(x)$  for all space-time points  $x$  and thus the energy density  $\varepsilon(x)$  in the local rest frame. In order to exclude contributions to  $T_{\mu\nu}$  from noninteracting nucleons in the initial phase all nucleons without prior interactions are discarded in the rapidity intervals  $[y_{tar} - 0.4, y_{tar} + 0.4]$  and  $[y_{pro} - 0.4, y_{pro} + 0.4]$  where  $y_{tar}$  and  $y_{pro}$  denote projectile and target rapidity, respectively. Note that the initial rapidity distributions of projectile and target nucleons are smeared out by about  $\pm 0.4$  due to Fermi motion.

In the actual calculation the initial grid has a dimension of  $1 \text{ fm} \times 1 \text{ fm} \times 1/\gamma_{cm} \text{ fm}$ , where  $\gamma_{cm}$  denotes the Lorentz  $\gamma$ -factor in the nucleon-nucleon center-of-mass system. After the time of maximum overlap  $t_m$  of the nuclei the grid-size in beam direction  $\Delta z_0 = 1/\gamma_{cm} \text{ [fm]}$  is increased linearly in time as  $\Delta z = \Delta z_0 + a(t - t_m)$ , where the parameter  $a$  is chosen in a way to keep the particle number in the local cells roughly constant during the longitudinal expansion of the system. In this way local fluctuations of the energy density  $\varepsilon(x)$  due to fluctuations in the particle number are kept low.

As an example we display in Fig. 2 the energy density  $\varepsilon(x, y = 0, z; t)$  for a



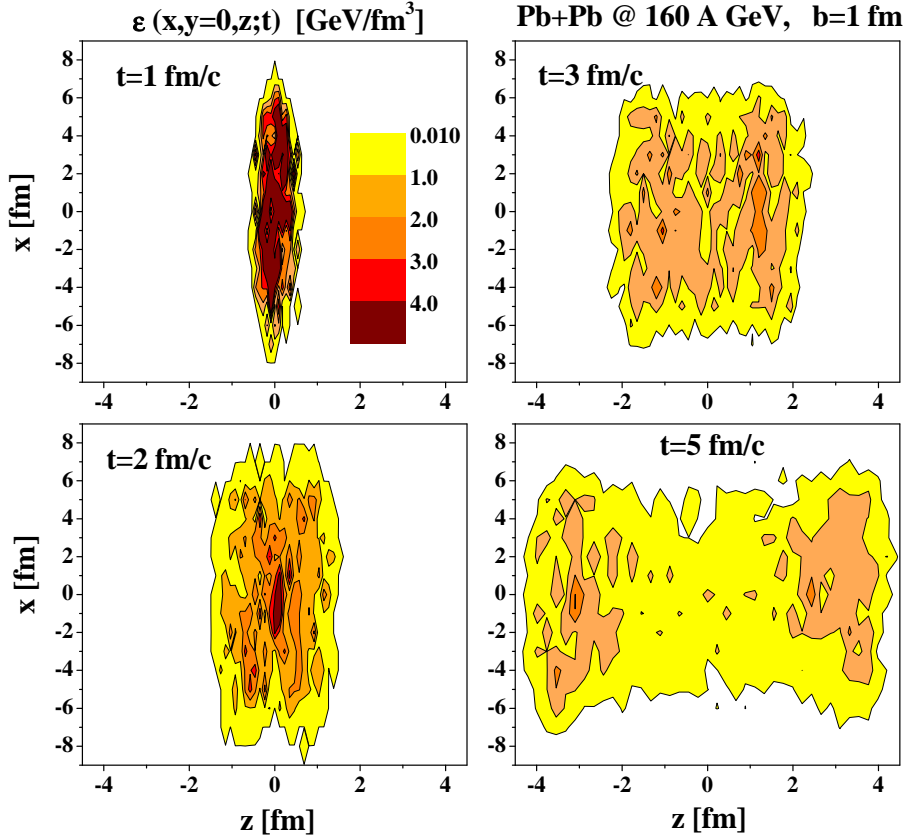


Fig. 2. The energy density  $\varepsilon(x, y = 0, z; t)$  from HSD for a Pb+Pb collision at 160 A·GeV and impact parameter  $b = 1$  fm in terms of contour lines (0.01, 1, 2, 3, 4 GeV/fm<sup>3</sup>) for times of 1, 2, 3 and 5 fm/c (from contact). Note that noninteracting nucleons have been discarded in the actual calculation of the energy-momentum tensor.

Pb+Pb collision at 160 A·GeV and impact parameter  $b = 1$  fm in terms of contour lines for times of 1, 2, 3 and 5 fm/c (from contact). It is clearly seen that energy densities above 4 GeV/fm<sup>3</sup> are reached in the early overlap phase of the reaction and that  $\varepsilon(x)$  drops within a few fm/c below 1 GeV/fm<sup>3</sup> in the center of the grid. On the other hand the energy density in the region of the leading particles - moving almost with the velocity of light - stays above 1 GeV/fm<sup>3</sup> due to Lorentz time dilatation since the time  $t$  here is measured in the nucleon-nucleon center-of-mass system. Note that in the local rest frame of the leading particles the eigentime  $\tau$  is roughly given  $\tau \approx t/\gamma_{cm}$  with  $\gamma_{cm} \approx 9.3$ .

Another view of the space time evolution of the energy density is given in Fig. 3 where we display  $\varepsilon(x = 0, y = 0, z; t)$  for the same system as in Fig. 2 on a linear scale. The contact time of the two Pb nuclei here is 2 fm/c and the overlap phase of the Lorentz contracted nuclei is identified by a sharp peak in space-time which is essentially given by the diameter of the nuclei divided by  $\gamma_{cm}$ . As noted before, the energy density in the center of the reaction volume ( $z \approx 0$ ) drops fast below 1 GeV/fm<sup>3</sup> whereas the ridges close to the lightcone basically stem from the leading ends of the strings formed in the early nucleon-

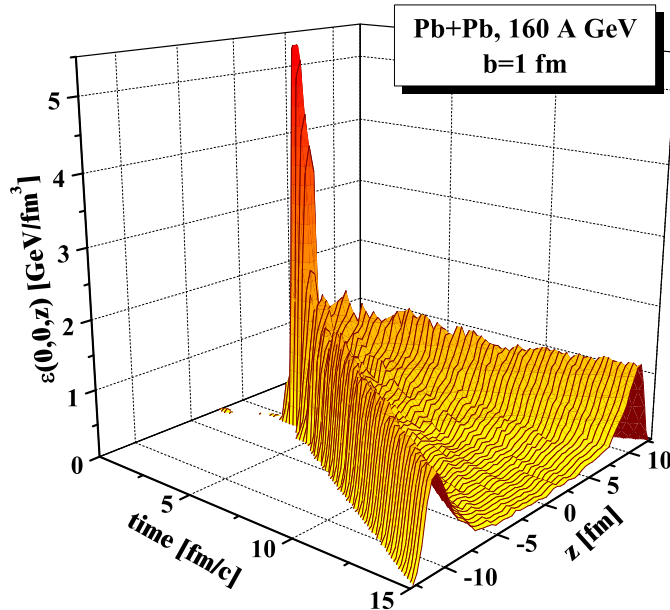


Fig. 3. The energy density  $\varepsilon(x = 0, y = 0, z; t)$  from HSD for a Pb+Pb collision at 160 A·GeV and impact parameter  $b = 1$  fm on a linear scale. Note that noninteracting nucleons have been discarded in the actual calculation of the energy-momentum tensor such that  $\varepsilon(x) \neq 0$  only after contact of the two Pb nuclei which is  $\sim 2$  fm/c.

nucleon collisions. In these space-time regions all reaction rates are reduced by the factor  $\sim 1/\gamma_{cm}$  such that the transport calculations have to be carried to large times of several hundred fm/c in order to catch the dynamics and decays in these regions. In the central regime, however, all interaction rates vanish after about 15 fm/c. Since the  $c, \bar{c}$  pairs are produced dominantly at midrapidity with a small spread in rapidity ( $\sigma_y \approx 0.8$  at 160 A·GeV) it is the central region that is of primary interest for this study.

Of further interest is the size of the total volume (measured in the nucleon-nucleon cms) with an energy density above a certain cut  $\varepsilon_c$ , *i.e.*

$$V(\varepsilon_c; t) := \int d^3r \Theta(\varepsilon(\mathbf{r}; t) - \varepsilon_c), \quad (11)$$

which quantifies the volume for charmonium dissolution as a function of time  $t$ . The corresponding information is displayed in Fig. 4 for  $\varepsilon_c = 1$  GeV/fm<sup>3</sup> (left part) and 1.5 GeV/fm<sup>3</sup> (right part) as a function of time for impact parameter  $b=1$  to 12 fm (in steps of  $\Delta b = 1$  fm). These volumina may be compared

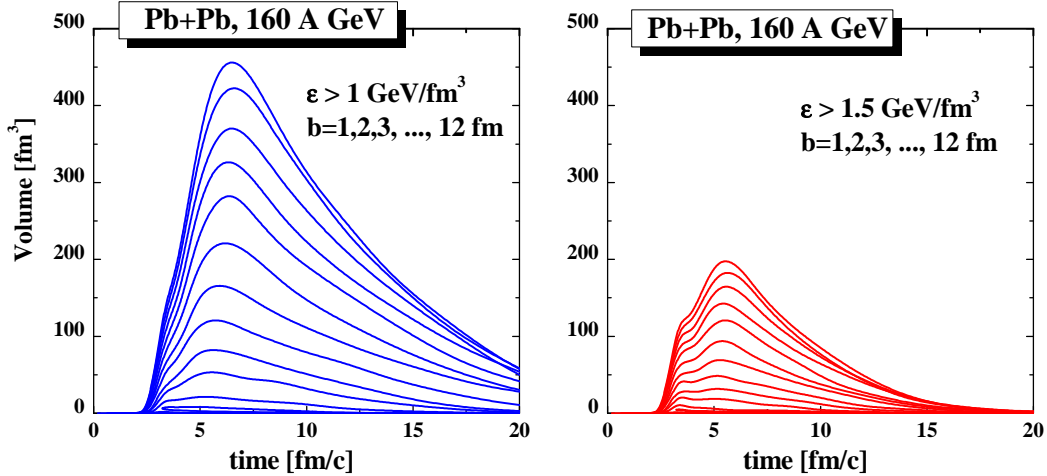


Fig. 4. The volume  $V(\varepsilon_c; t)$  (11) from HSD for Pb+Pb collisions at 160 A·GeV and impact parameter  $b = 1, 2, \dots, 12$  fm for  $\varepsilon > \varepsilon_c = 1$  GeV/fm<sup>3</sup> (left part) and  $\varepsilon > \varepsilon_c = 1.5$  GeV/fm<sup>3</sup> (right part).

to the Lorentz contracted eigenvolume of a Pb nucleus that is about 160 fm<sup>3</sup> in the cms. It is clearly seen that hadron formation and the explosion (or expansion) of the system lead to larger volumina  $V(\varepsilon_c; t)$  in central reactions especially for  $\varepsilon_c = 1$  GeV/fm<sup>3</sup>. Note, however, that charmonia dynamically cannot explore the whole volume displayed in Fig. 4, since this volume is dominated by the space-time regimes close to the lightcone (*cf.* Fig. 3), where practically no charmonia appear at 160 A·GeV.

The ‘threshold scenario’ for charmonium dissociation now is implemented in a straight forward way: whenever the local energy density  $\varepsilon(x)$  is above a threshold value  $\varepsilon_j$ , where the index  $j$  stands for  $J/\Psi$ ,  $\chi_c$ ,  $\Psi'$ , the charmonium is fully dissociated to  $c + \bar{c}$ . The default threshold energy densities adopted are  $\varepsilon_1 = 16$  GeV/fm<sup>3</sup> for  $J/\Psi$ ,  $\varepsilon_2 = 2$  GeV/fm<sup>3</sup> for  $\chi_c$ , and  $\varepsilon_3 = 2$  GeV/fm<sup>3</sup> for  $\Psi'$ . The reformation of charmonia at the phase boundary to the hadronic system is discarded in view of the very low charm quark density at SPS energies.

### 3 Comparison to data

We directly step on with results for the charmonium suppression at SPS energies in comparison with the experimental data from the NA50 and NA60 Collaborations. These Collaborations present their results on  $J/\Psi$  suppression as the ratio of the dimuon decay of  $J/\Psi$  relative to the Drell-Yan background from 2.9 - 4.5 GeV invariant mass as a function of the transverse energy  $E_T$ , or alternative, as a function of the number of participants  $N_{\text{part}}$ , *i.e.*

$$B_{\mu\mu}\sigma(J/\Psi)/\sigma(DY)|_{2.9-4.5}, \quad (12)$$

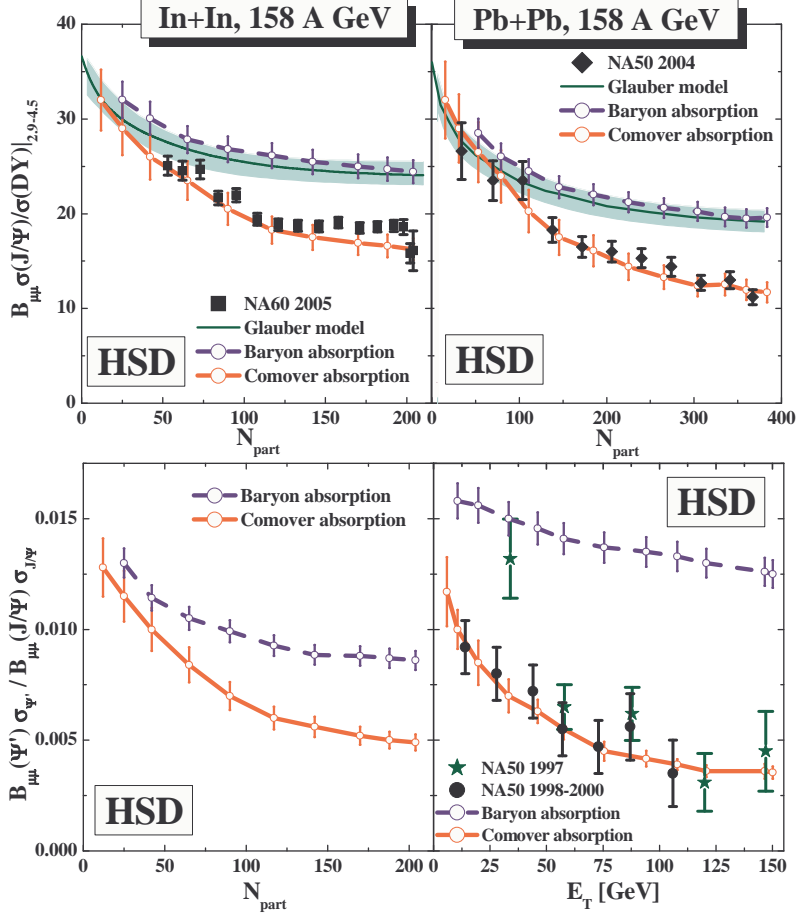


Fig. 5. The ratio  $B_{\mu\mu}\sigma(J/\Psi)/\sigma(DY)$  as a function of the number of participants in In+In (l.h.s.) and Pb+Pb reactions (r.h.s.) at 158 A·GeV. The full symbols denote the data from the NA50 and NA60 Collaborations (from Refs. [17,18,61]), while the dashed (blue) lines represent the HSD calculations including only dissociation channels with nucleons. The lower parts of the figure show the HSD results in the same limit for the  $\Psi'$  to  $J/\Psi$  ratio as a function of  $N_{part}$  (for In+In) or the transverse energy  $E_T$  (for Pb+Pb). The solid (red) lines show the HSD results for the comover absorption model with a matrix element squared  $|M_0|^2 = 0.18 \text{ fm}^2/\text{GeV}^2$ . The (light blue) bands in the upper parts of the figure give the estimate for the normal nuclear  $J/\Psi$  absorption as calculated by the NA60 Collaboration. The vertical lines on the graphs reflect the theoretical uncertainty due to limited statistics of the calculations.

where  $B_{\mu\mu}$  is the branching ratio for  $J/\Psi \rightarrow \mu^+\mu^-$ .

In the theoretical approaches we calculate the  $J/\Psi$  survival probability  $S_{J/\Psi}$  defined as

$$S_{J/\Psi} = \frac{N_{fin}^{J/\Psi}}{N_{BB}^{J/\Psi}}, \quad (13)$$

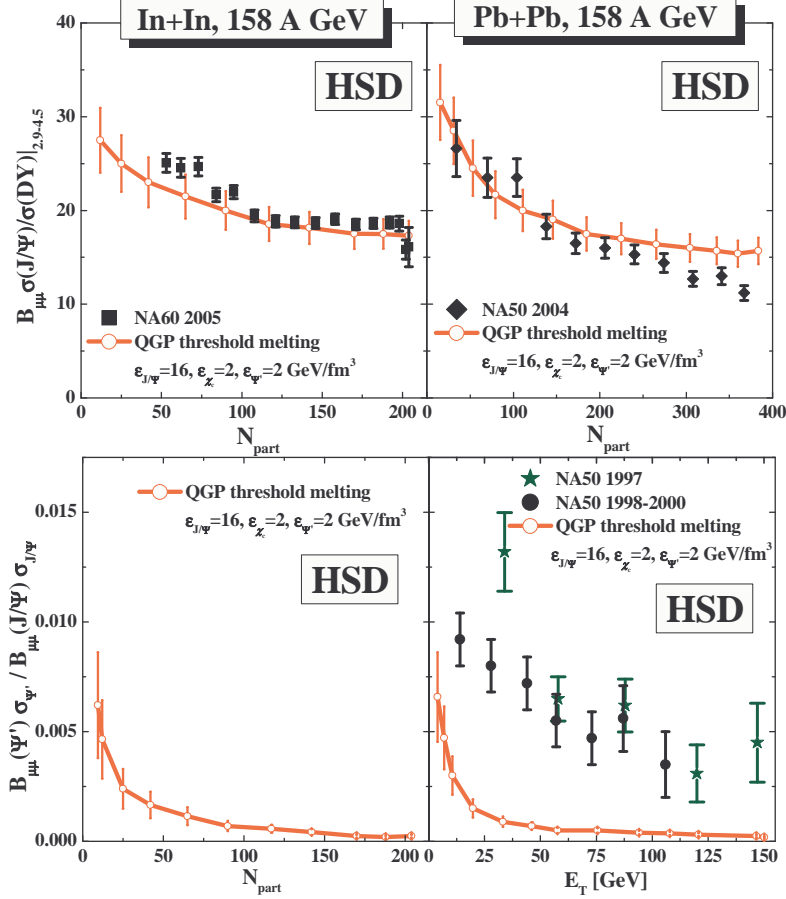


Fig. 6. Same as Fig. 5 but for the ‘QGP threshold scenario’ with  $\varepsilon_{J/\Psi} = 16 \text{ GeV}/\text{fm}^3$ ,  $\varepsilon_{\chi_c} = 2 \text{ GeV}/\text{fm}^3 = \varepsilon_{\Psi'}$  while discarding comover absorption, *i.e.* for  $|M_0|^2 = 0$ .

where  $N_{fin}^{J/\Psi}$  and  $N_{BB}^{J/\Psi}$  denote the final number of  $J/\Psi$  mesons and the number of  $J/\Psi$ 's produced initially by  $BB$  reactions, respectively. In order to compare our calculated results to experimental data we need an extra input, *i.e.* the normalization factor  $B_{\mu\mu}\sigma_{NN}(J/\Psi)/\sigma_{NN}(DY)$ , which defines the  $J/\Psi$  over Drell-Yan ratio for elementary nucleon-nucleon collisions. We choose  $B_{\mu\mu}\sigma_{NN}(J/\Psi)/\sigma_{NN}(DY) = 36$  in line with the NA60 compilation [18].

Furthermore, the  $\Psi'$  suppression is presented experimentally by the ratio

$$\frac{B_{\mu\mu}(\Psi' \rightarrow \mu\mu)\sigma(\Psi')/\sigma(DY)}{B_{\mu\mu}(J/\Psi \rightarrow \mu\mu)\sigma(J/\Psi)/\sigma(DY)}. \quad (14)$$

In our calculations we adopt this ratio to be 0.0165 for nucleon-nucleon collisions, which is again based on the average over  $pp, pd, pA$  reactions [45].

In order to investigate the anomalous charmonium suppression in nucleus-nucleus collisions we first show in Fig. 5 the calculated ratio  $B_{\mu\mu}\sigma(J/\Psi)/\sigma(DY)$  as a function of  $N_{part}$  for Pb+Pb and In+In collisions at 158 A·GeV (upper

plots) in the nuclear suppression scenario, i.e. without comover dissociation or ‘QGP threshold suppression’. The dashed (blue) lines stand for the HSD result while the (light blue) bands give the estimate for the normal nuclear  $J/\Psi$  absorption as calculated by the NA60 Collaboration. The normal nuclear suppression from HSD is seen to be slightly lower than the (model dependent) estimate from NA60, however, agrees quite well with their model calculations for more central reactions. The various experimental data points have been taken from Refs. [17,18,61]. It is clearly seen that the charmonium dissociation with only nucleons is insufficient to describe the data for both systems. In the lower part of Fig. 5 we compare the calculated ratio  $\Psi'$  over  $J/\Psi$  as a function of  $N_{part}$  (for In+In reactions) or the transverse energy  $E_T$  (for Pb+Pb collisions), respectively, in comparison to the data available. The Pb+Pb data demonstrate that the centrality dependence as well as the absolute ratio cannot be explained by nuclear dissociation channels alone which is a well known fact in the community.

Apart from the statistical uncertainties in the calculations - reflected by the vertical lines on the theoretical graphs in Fig. 5 - some dependence on the model parameters enters the actual numbers in Fig. 5. The charmonium nuclear absorption cross section is considered to be ‘fixed’ by the NA50/NA60 compilations and we have taken the same cross section for the ‘pre-resonance’ cross section for the  $J/\Psi$  and  $\chi_c$ . Accordingly the life-time of the pre-resonance state ( $\tau_{c\bar{c}} = 0.3$  fm/c) has no impact on the absorption with baryons as far as the  $J/\Psi$  and  $\chi_c$  mesons are concerned. Only for  $\Psi'$  collisions with baryons this plays a role since the  $\Psi' +$  baryon cross section is larger (7.6 mb). Consequently the  $J/\Psi$  suppression (including the feed down from  $\chi_c$ ) does not depend on  $\tau_{c\bar{c}}$ . The finite life-time, however, plays a role for  $\Psi'$  suppression as can be seen in the lower right part of Fig. 5 since it leads to a larger baryon absorption of  $\Psi'$  (relative to  $J/\Psi$ ) with increasing centrality by about 22%. According to our understanding the life-time of 0.3 fm/c is a lower limit (in line with the Heisenberg uncertainty relation); it leads to a maximum suppression of  $\Psi'$  relative to  $J/\Psi$  with centrality. On the other hand, a very large life-time  $\tau_{c\bar{c}}$  will lead to a constant ratio of  $\Psi'$  to  $J/\Psi$  with centrality since only the pre-resonance cross section will apply. Accordingly, the  $\Psi'$  to  $J/\Psi$  ratio is driven by the value of  $\tau_{c\bar{c}}$  since the ratio of the dissociation cross section for the formed mesons is fixed by the ratio of their mean square radii. However, independently on the life-time  $\tau_{c\bar{c}}$  of the pre-resonance state the experimental data will be badly missed for the  $\Psi'$  to  $J/\Psi$  ratio if only baryon dissociation is included, because the case considered here already provides a maximum suppression of the  $\Psi'$  for interactions with baryons.

As a next step we add the comover dissociation channels within the model described in Section 2.1 for a matrix element squared  $|M_0|^2 = 0.18$  fm<sup>2</sup>/GeV<sup>2</sup>. Note that in this case the charmonium reformation channels are incorporated, too, but could be discarded since the charmonium regeneration is negligible at

SPS energies (*cf.* Ref. [35]). The extra suppression of charmonia by comovers is seen in Fig. 5 (solid (red) lines) to match the  $J/\Psi$  suppression in In+In and Pb+Pb as well as the  $\Psi'$  to  $J/\Psi$  ratio (for Pb+Pb) rather well. The more recent data (1998-2000) for the  $\Psi'$  to  $J/\Psi$  ratio agree with the HSD prediction within error bars. This had been a problem in the past when comparing to the 1997 data (dark green stars). We conclude that the comover absorption model presently cannot be ruled out on the basis of the available data sets within error bars. The  $\Psi'$  to  $J/\Psi$  ratio for In+In versus centrality is not yet available from the experimental side but the theoretical predictions are provided in Fig. 5 and might be approved/falsified in near future.

Some comments to the comover absorption model appear in place: As shown in Fig. 7.2 of Ref. [19] the comover densities in central Pb+Pb collisions at 158 A·GeV become quite large and almost reach  $2/\text{fm}^3$  in the maximum which appears high for ‘free’ mesons with an eigenvolume of about  $1 \text{ fm}^3$ . However, the quasi-particle mesons considered here dynamically should not be identified with ‘free’ meson states that show a long polarization tail in the vacuum. As known from lattice QCD the correlators for pions and  $\rho$ -mesons survive well above the critical temperature  $T_c$ , such that ‘dressed’ mesons, i.e spectral densities with the quantum numbers of the pseudo-scalar and vector (isovector) modes, also show up at high energy density (similar to the  $J/\Psi$  discussed above [6,7,8]). Such ‘dressed’ mesons are expected to have a shorter polarization tail - since the reference vacuum has changed and the vacuum polarization decreases - and thus are much smaller in size. In any case, these ‘states’ (or resonances) will dissociate charmonia by a quark rearrangement interaction in exchanging a light quark with a  $c$  or  $\bar{c}$  quark.

The results for the ‘threshold scenario’ are displayed in Fig. 6 in comparison to the same data for the thresholds  $\varepsilon_{J/\Psi} = 16 \text{ GeV}/\text{fm}^3$ ,  $\varepsilon_{\chi_c} = 2 \text{ GeV}/\text{fm}^3 = \varepsilon_{\Psi'}$  while discarding any dissociation with comovers, i.e.  $|M_0|^2 = 0$ . In this scenario the  $J/\Psi$  suppression is well described for In+In but the suppression is slightly too weak for very central Pb+Pb reactions. This result emerges since practically all  $\chi_c$  and  $\Psi'$  dissolve for  $N_{part} > 100$  in both systems whereas the  $J/\Psi$  itself survives at the energy densities reached in the collision. Since the nucleon dissociation is a flat function of  $N_{part}$  for central reactions the total absorption strength is flat, too. The deviations seen in Fig. 6 might indicate a partial melting of the  $J/\Psi$  for  $N_{part} > 250$ , which is not in line with the lattice QCD calculations claiming at least  $\varepsilon_{J/\Psi} > 5 \text{ GeV}/\text{fm}^3$ . In fact, a lower threshold of  $5 \text{ GeV}/\text{fm}^3$  (instead of  $16 \text{ GeV}/\text{fm}^3$ ) for the  $J/\Psi$  has practically no effect on the results shown in Fig. 6. Furthermore, a threshold energy density of  $2 \text{ GeV}/\text{fm}^3$  for the  $\Psi'$  leads to a dramatic reduction of the  $\Psi'$  to  $J/\Psi$  ratio which is in severe conflict with the data (lower part of Fig. 6). Also note that due to energy density fluctuations in reactions with fixed  $N_{part}$  (or  $E_T$ ) there is no step in the suppression of  $J/\Psi$  versus centrality as pointed out before by Gorenstein et al. in Ref. [73].

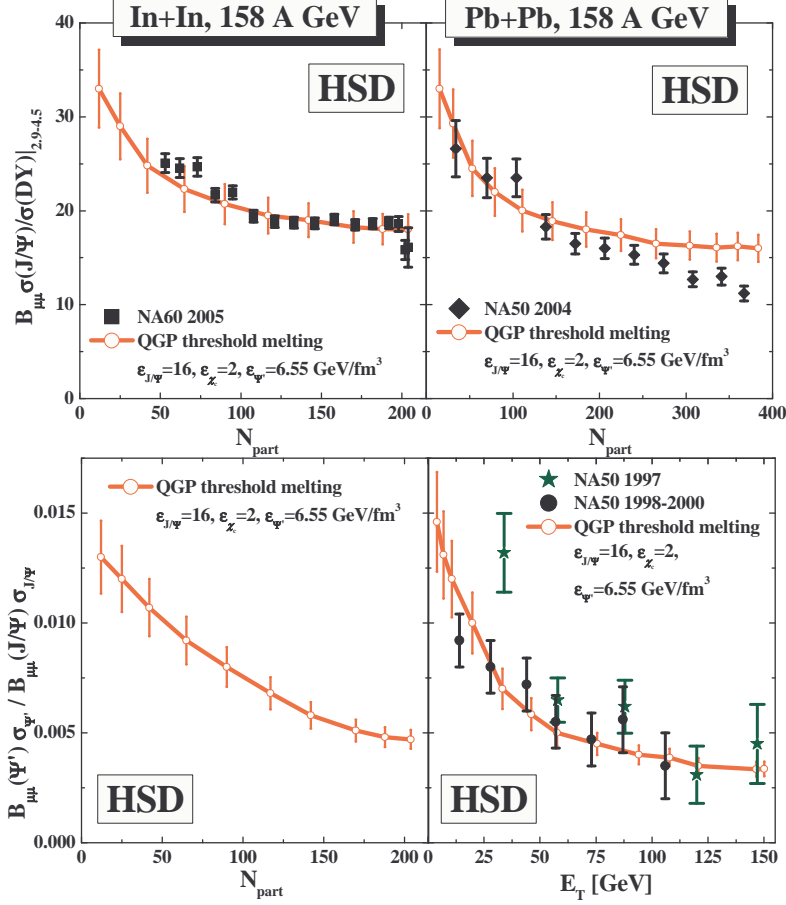


Fig. 7. Same as Fig. 5 but for the ‘QGP threshold scenario’ with  $\varepsilon_{J/\Psi} = 16 \text{ GeV/fm}^3$ ,  $\varepsilon_{\chi_c} = 2 \text{ GeV/fm}^3$ ,  $\varepsilon_{\Psi'} = 6.55 \text{ GeV/fm}^3$  while discarding comover absorption, *i.e.* for  $|M_0|^2 = 0$ .

Since in the ‘threshold scenario’ the  $J/\Psi$  suppression is rather well accounted for by the melting of the  $\chi_c$  it might be tempting to ‘extract’ a dissociation energy density for the  $\Psi'$  via the  $\Psi'$  to  $J/\Psi$  ratio. This may indeed be achieved for  $\varepsilon_{\Psi'} = 6.55 \text{ GeV/fm}^3$  as shown in Fig. 7 where now also the  $\Psi'$  to  $J/\Psi$  ratio is well reproduced for Pb+Pb. Respective predictions for In+In within this scenario are presented in the lower left part of Fig. 7 and wait for confirmation or disproof. We recall, however, that the energy density of  $6.55 \text{ GeV/fm}^3$  for  $\Psi'$  dissociation is not supported by present lattice calculations such that this limit should be ruled out.

As the last model scenario we assume that both  $J/\Psi$  and  $\Psi'$  are practically not dissociated in nucleus-nucleus reactions at SPS energies but let the  $\chi_c$  melt above  $2 \text{ GeV/fm}^3$  as before. In this case one may estimate the maximum suppression by comovers that is compatible with the data. This combined scenario allows to fix a matrix element squared  $|M_0|^2 \approx 0.09 \text{ fm}^2/\text{GeV}^2$  that gives results still compatible with the  $J/\Psi$  suppression for In+In and Pb+Pb (solid lines in Fig. 8). The dashed lines in Fig. 8 show the results without any



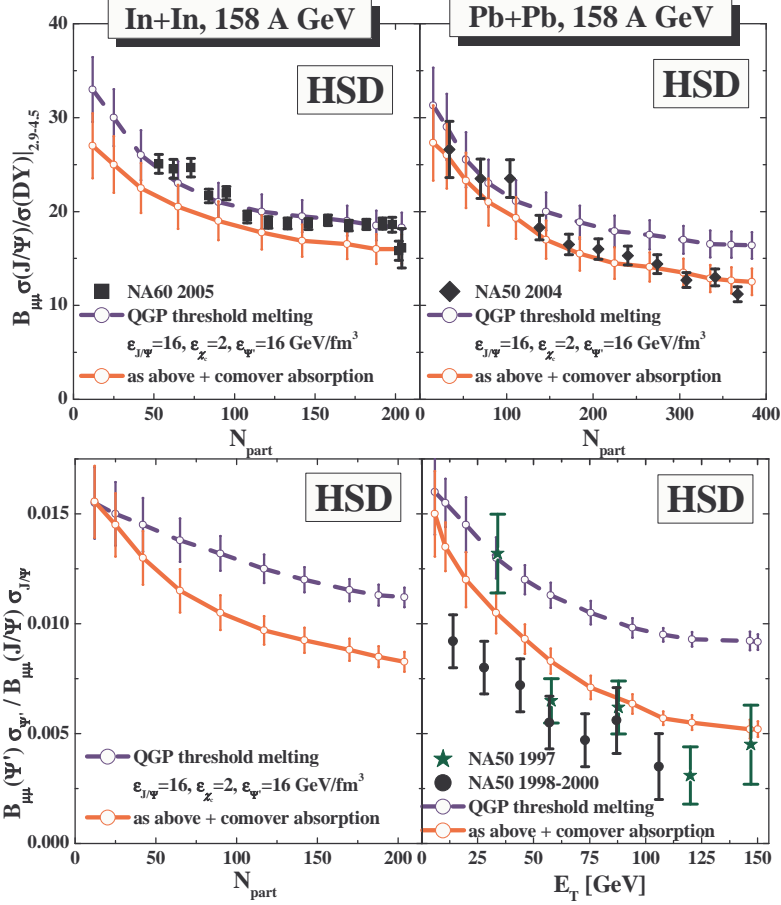


Fig. 8. Same as Fig. 5 but for the ‘QGP threshold scenario’ with  $\varepsilon_{J/\Psi} = 16 \text{ GeV}/\text{fm}^3$ ,  $\varepsilon_{\chi_c} = 2 \text{ GeV}/\text{fm}^3$ ,  $\varepsilon_{\Psi'} = 16 \text{ GeV}/\text{fm}^3$  (dashed blue lines) and with additional comover absorption for  $|M_0|^2 = 0.09 \text{ fm}^2/\text{GeV}^2$  (red solid lines).

comover absorption and are due to the melting of the  $\chi_c$  above  $2 \text{ GeV}/\text{fm}^3$  alone. However, in this combined approach the  $\Psi'$  to  $J/\Psi$  ratio turns out to be systematically too high in comparison to the data for Pb+Pb such that this scenario should be ruled out, too, in particular with respect to the extreme threshold for  $\Psi'$  dissociation.

Since the NA60 Collaboration prefers to represent their data in a model dependent way by plotting their experimental results relative to the normal nuclear absorption model we additionally show in Fig. 9 our calculations for In+In (red lines with open squares) and Pb+Pb (blue lines with open circles) as a function of the number of participants  $N_{part}$  relative to the normal nuclear absorption given by the straight black line (according to the NA60 compilation). The full dots and squares denote the respective data from the NA50 and NA60 Collaborations. The model calculations reflect the comover absorption model (right part) and the ‘QGP threshold scenario’ (left part) with  $\varepsilon_{J/\Psi} = 16 \text{ GeV}/\text{fm}^3$ ,  $\varepsilon_{\chi_c} = 2 \text{ GeV}/\text{fm}^3$ ,  $\varepsilon_{\Psi'} = 6.55 \text{ GeV}/\text{fm}^3$ . Since only the representation is different the message stays the same: The comover absorp-

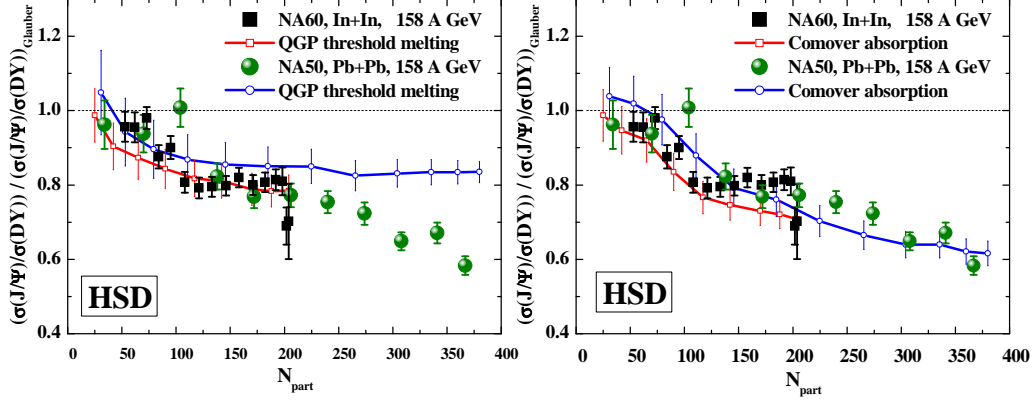


Fig. 9. The ratio  $B_{\mu\mu}\sigma(J/\Psi)/\sigma(DY)$  as a function of the number of participants  $N_{part}$  in In+In (red line with open squares) and Pb+Pb reactions (blue line with open circles) at 158 A·GeV relative to the normal nuclear absorption given by the straight black line. The full dots and squares denote the respective data from the NA50 and NA60 Collaborations. The model calculations reflect the comover absorption model (right part) and the ‘QGP threshold scenario’ (left part) with  $\varepsilon_{J/\Psi} = 16$  GeV/fm<sup>3</sup>,  $\varepsilon_{\chi_c} = 2$  GeV/fm<sup>3</sup>,  $\varepsilon_{\Psi'} = 6.55$  GeV/fm<sup>3</sup> while discarding comover absorption.

tion model follows slightly better the fall of the  $J/\Psi$  survival probability with increasing centrality whereas the ‘threshold scenario’ leads to an approximate plateau in both reactions for high centrality.

#### 4 Predictions for FAIR energies

The CBM Collaboration at GSI is aiming at charmonium measurements at the future FAIR facility [74]. This opens up the possibility to explore the charmonium suppression mechanism at lower bombarding energies of about 25 A·GeV in Au+Au collisions. First predictions for central reactions within the comover model have been reported in Ref. [22]. Here we extend the earlier studies to the full centrality dependence of the  $J/\Psi$  suppression also within the ‘threshold scenario’ and additionally provide predictions for the  $\Psi'$  to  $J/\Psi$  ratio. The corresponding HSD results are displayed in Fig. 10 for the survival probability  $S_{J/\Psi}$  (left plot) and ratio  $\Psi'$  to  $J/\Psi$  (right plot) as a function of the number of participants  $N_{part}$ . The blue lines reflect the ‘threshold scenario’ for  $\varepsilon_{J/\Psi} = 16$  GeV/fm<sup>3</sup>,  $\varepsilon_{\chi_c} = 2$  GeV/fm<sup>3</sup>,  $\varepsilon_{\Psi'} = 6.55$  GeV/fm<sup>3</sup> while the violet line stands for the ‘threshold scenario’ with a more realistic value of  $\varepsilon_{\Psi'}$ , i.e.  $\varepsilon_{J/\Psi} = 16$  GeV/fm<sup>3</sup>,  $\varepsilon_{\chi_c} = 2$  GeV/fm<sup>3</sup>,  $\varepsilon_{\Psi'} = 2$  GeV/fm<sup>3</sup>. The solid red lines denote the results for the comover absorption model with the standard matrix element squared  $|M_0|^2 = 0.18$  fm<sup>2</sup>/GeV<sup>2</sup>.

We note that in Au+Au reactions at 25 A·GeV the standard nuclear suppres-

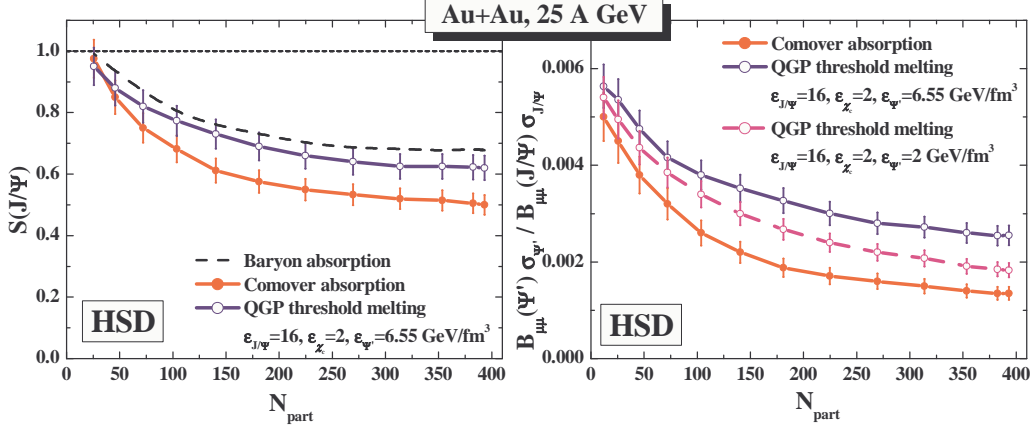


Fig. 10. The survival probability  $S_{J/\Psi}$  (left plot) and ratio  $\Psi'$  to  $J/\Psi$  (right plot) as a function of the number of participants  $N_{part}$  in Au+Au reactions at 25 A·GeV. The blue lines (with open dots) reflect the ‘threshold scenario’ for  $\epsilon_{J/\Psi} = 16$  GeV/fm<sup>3</sup>,  $\epsilon_{\chi_c} = 2$  GeV/fm<sup>3</sup>,  $\epsilon_{\Psi'} = 6.55$  GeV/fm<sup>3</sup> while the violet line (the lower line with open dots on the r.h.s.) stands for the ‘threshold scenario’ for  $\epsilon_{J/\Psi} = 16$  GeV/fm<sup>3</sup>,  $\epsilon_{\chi_c} = 2$  GeV/fm<sup>3</sup>,  $\epsilon_{\Psi'} = 2$  GeV/fm<sup>3</sup>. The solid red lines (full dots) denote the results for the comover absorption model with the standard matrix element squared  $|M_0|^2 = 0.18$  fm<sup>2</sup>/GeV<sup>2</sup>. The dashed line (l.h.s.) represents the HSD calculations including only dissociation channels with nucleons.

sion of  $J/\Psi$  (dashed line in the left plot) almost coincides with the ‘threshold scenario’ (solid line with open dots in the left plot) since only a very low amount of  $\chi_c$  and no  $J/\Psi$  are melted at the energy densities reached in these reactions. On the other hand the comover density decreases only moderately when stepping down in energy from 158 A·GeV to 25 A·GeV such that the  $J/\Psi$  survival probability in the comover absorption model (lower solid line in the left part) is substantially lower. This also holds for the  $\Psi'$  to  $J/\Psi$  ratio versus centrality where even a lower threshold  $\epsilon_{\Psi'} = 2$  GeV/fm<sup>3</sup> leads to a ratio (middle line in the right part) that is clearly above the result achieved in the comover absorption model (lower line in the right part). Consequently the different dissociation scenarios may well be distinguished in future charmonium measurements at FAIR.

## 5 Summary

In summarizing this work we have found that present data on charmonium suppression for Pb+Pb and In+In reactions at top SPS energies compare well with microscopic transport calculations in the comover model involving only a single parameter for the average matrix element squared  $|M_0|^2$  that fixes the strength of the charmonium cross sections with comovers. This holds for the  $J/\Psi$  suppression as well as the  $\Psi'$  to  $J/\Psi$  ratio versus collision centrality. The

bare ‘QGP threshold scenario’ gives satisfying results for the  $J/\Psi$  suppression for both systems at 158 A·GeV but fails in the  $\Psi'$  to  $J/\Psi$  ratio since too many  $\Psi'$  already melt away for a critical energy density of 2 GeV/fm<sup>3</sup> at 158 A·GeV. Only when assuming the  $\Psi'$  to dissolve above  $\sim 6.5$  GeV/fm<sup>3</sup> a reasonable description of all data is achieved in the ‘QGP threshold scenario’; this threshold, however, is not in accordance with present lattice QCD calculations such that the ‘threshold scenario’ meets severe problems. This also holds for a combined model including ‘threshold melting’ and reduced ‘comover absorption’ as shown in Section 3.

On the other hand the different scenarios can clearly be distinguished at FAIR energies (of about 25 A·GeV) where the centrality dependence of the  $J/\Psi$  survival probability and the  $\Psi'$  to  $J/\Psi$  ratio are significantly lower in the comover absorption model. This result comes about since the average comover density decreases only moderately with lower bombarding energy whereas the region in space-time with energy densities above critical values of *e.g.* 2 GeV/fm<sup>3</sup> decreases rapidly and ceases to exist below about 20 A·GeV even in central collisions. This ideally might open up the possibility to measure excitation functions of the  $J/\Psi$  survival probability and the  $\Psi'$  to  $J/\Psi$  ratio in central Au+Au collisions, where clear steps would indicate the presence of ‘melting thresholds’ whereas a smooth excitation function would be in favor of the comover absorption approach.

## Acknowledgement

The authors acknowledge inspiring discussions with A. Kostyuk, E. Scomparin and P. Senger.

## References

- [1] *Quark Matter 2005*, Nucl. Phys. A 774 (2006) 1.
- [2] T. Matsui and H. Satz, Phys. Lett. B 178 (1986) 416.
- [3] H. Satz, Rep. Progr. Phys. 63 (2000) 1511.
- [4] H. Satz, J. Phys. G 32 (2006) R25.
- [5] F. Karsch, D. Kharzeev, and H. Satz, Phys. Lett. B **637** (2006) 75.
- [6] S. Datta, F. Karsch, P. Petreczky, and I. Wetzorke, J. Phys. G 30 (2004) S1347.
- [7] M. Asakawa and T. Hatsuda, J. Phys. G 30 (2004) S1337.

- [8] F. Karsch, J. Phys. G 30 (2004) S887.
- [9] H. van Hees and R. Rapp, Phys. Rev. C 71 (2005) 034907.
- [10] D. Kharzeev, C. Lourenco, M. Nardi, and H. Satz, Z. Phys. C 74 (1997) 307.
- [11] N. Armesto and A. Capella, Phys. Lett. B 430 (1998) 23;  
N. Armesto, A. Capella and E. G. Ferreira, Phys. Rev. C 59 (1999) 395. A.  
Capella, E. G. Ferreira, and A. B. Kaidalov, Phys. Rev. Lett. 85 (2000) 2080.
- [12] J. P. Blaizot and J. Y. Ollitrault, Phys. Rev. Lett. 77 (1996) 1703;  
J. P. Blaizot, P.M. Dinh and J. Y. Ollitrault, *ibid.* 85 (2000) 4012.
- [13] M. C. Abreu *et al.*, NA50 Collaboration, Phys. Lett. B 410 (1997) 337.
- [14] M. C. Abreu *et al.*, NA50 Collaboration, Phys. Lett. B 477 (2000) 28.
- [15] M. C. Abreu *et al.*, NA50 Collaboration, Phys. Lett. B 450 (1999) 456.
- [16] M. C. Abreu *et al.*, NA38 Collaboration, Phys. Lett. B 449, 128 (1999).
- [17] B. Alessandro *et al.*, NA50 Collaboration, Eur. Phys. J. C 39 (2005) 335.
- [18] A. Foerster *et al.*, NA60 Collaboration, arXiv:nucl-ex/0609039.
- [19] W. Cassing and E. L. Bratkovskaya, Phys. Rep. 308 (1999) 65.
- [20] R. Vogt, Phys. Rep. 310 (1999) 197.
- [21] C. Gerschel and J. Hüfner, Ann. Rev. Nucl. Part. Sci. 49 (1999) 255.
- [22] W. Cassing, E. L. Bratkovskaya, and S. Juchem, Nucl. Phys. A 674 (2000) 249.
- [23] D. E. Kahana and S. H. Kahana, Prog. Part. Nucl. Phys. 42 (1999) 269.
- [24] C. Spieles, R. Vogt, L. Gerland, S. A. Bass, M. Bleicher, H. Stöcker, and W. Greiner, J. Phys. G 25, 2351 (1999). Phys. Rev. C 60 (1999) 054901.
- [25] L. Gerland, L. Frankfurt, M. Strikman, H. Stöcker, and W. Greiner, Nucl. Phys. A 663 (2000) 1019.
- [26] K. L. Haglin, Phys. Rev. C 61 (2000) 031903;  
K. L. Haglin and C. Gale, Phys. Rev. C 63 (2001) 065201.
- [27] Z. Lin and C. M. Ko, Phys. Rev. C 62 (2000) 034903.
- [28] Z. Lin and C. M. Ko, J. Phys. G 27 (2001) 617.
- [29] A. Sibirtsev, K. Tsushima, and A. W. Thomas, Phys. Rev. C 63 (2001) 044906;  
A. Sibirtsev, K. Tsushima, K. Saito, and A. W. Thomas, Phys. Lett. B 484 (2000) 23.
- [30] B. Müller, Nucl. Phys. A 661 (1999) 272c.
- [31] B. Zhang, C. M. Ko, B.-A. Li, Z. Lin, B.-H. Sa, Phys. Rev. C 62 (2000) 054905.

- [32] L. Grandchamp and R. Rapp, Phys. Lett. B 523 (2001) 60; Nucl. Phys. A 709 (2002) 415.
- [33] D. Blaschke, Y. Kalinovsky and V. Yudin, Lect. Notes Phys. **647** (2004) 366.
- [34] M. Bedjidian *et al.*, arXiv:hep-ph/0311048.
- [35] E. L. Bratkovskaya, W. Cassing, and H. Stöcker, Phys. Rev. C 67 (2003) 054905.
- [36] H. Büsching *et al.*, PHENIX Collaboration, Nucl. Phys. A 774 (2006) 103.
- [37] A. Capella and E. Ferreira, Eur. Phys. J. C 42 (2005) 419.
- [38] R. Rapp, Eur. Phys. J. C 43 (2005) 91.
- [39] S. Digal, S. Fortunato and H. Satz, Eur. Phys. J. C 32 (2004) 547.
- [40] W. Cassing, E. L. Bratkovskaya, and A. Sibirtsev, Nucl. Phys. A 691 (2001) 753.
- [41] E. L. Bratkovskaya, A. P. Kostyuk, W. Cassing, and H. Stöcker, Phys. Rev. C 69 (2004) 054903.
- [42] H. Weber, E.L. Bratkovskaya, W. Cassing, and H. Stöcker, Phys. Rev. C 67 (2003) 014904; E. L. Bratkovskaya, M. Bleicher, M. Reiter *et al.*, Phys. Rev. C 69 (2004) 054907.
- [43] L. Antoniazzi *et al.*, E705 Collaboration, Phys. Rev. Lett. 70 (1993) 383.
- [44] Y. Lemoigne *et al.*, WA11 Collaboration, Phys. Lett. B 113 (1982) 509.
- [45] B. Alessandro *et al.*, NA50 Collaboration, Phys. Lett. B 553 (2003) 167.
- [46] K. Hagiwara *et al.*, (Review of Particle Properties), Phys. Rev. D 66 (2002) 010001.
- [47] J. Geiss, W. Cassing, and C. Greiner, Nucl. Phys. A 644 (1998) 107.
- [48] M. Aguilar-Benitez *et al.*, NA16 Collaboration, Phys. Lett. B 135 (1984) 237.
- [49] M. Aguilar-Benitez *et al.*, NA27 Collaboration, Z. Phys. C 40 (1988) 321.
- [50] R. Ammar *et al.*, E743 Collaboration, Phys. Rev. Lett 61 (1988) 2185.
- [51] K. Kodama *et al.*, E653 Collaboration, Phys. Lett. B 263 (1991) 573; *ibid.* B 284 (1992) 461.
- [52] M. J. Leitch *et al.*, E789 Collaboration, Phys. Rev. Lett. 72 (1994) 2542.
- [53] S. Barlag *et al.*, NA32 Collaboration, Z. Phys. C 39 (1988) 451; *ibid.* C 49 (1991) 555; Phys. Lett. B 247 (1990) 113.
- [54] G. A. Alves *et al.*, E769 Collaboration, Phys. Rev. Lett. 77 (1996) 2388; *ibid.* 2392.

- [55] M. Adamovich et al., WA92 Collaboration, Nucl. Phys. B 495 (1997) 3.
- [56] E. M. Aitala et al., E791 Collaboration, Eur. Phys. J. C 4 (1999) 1.
- [57] S. S. Adler *et al.*, PHENIX Collaboration, Phys. Rev. Lett. 92 (2004) 051802; *ibid.* 96 (2006) 012304; hep-ex/0609032.
- [58] V. Abramov *et al.*, E672/E706 Collaboration, FERMILAB-Pub-91/62-E, IFVE-91-9, Mar. 1991.
- [59] B. Alessandro *et al.*, NA50 Collaboration, nucl-ex/0612012.
- [60] D. Kharzeev and R. L. Thews, Phys. Rev. C 60 (1999) 041901.
- [61] B. Alessandro *et al.*, NA50 Collaboration, nucl-ex/0612013.
- [62] P. Braun-Munzinger and J. Stachel, Phys. Lett. B 490 (2000) 196; Nucl. Phys. A 690 (2001) 119c.
- [63] R. L. Thews, M. Schroedter, and J. Rafelski, Phys. Rev. C 63 (2001) 054905.
- [64] P. Braun-Munzinger and K. Redlich, Eur. Phys. J. C 16 (2000) 519; Nucl. Phys. A661 (1999) 546.
- [65] K. Martins, D. Blaschke, and E. Quack, Phys. Rev. C 51 (1995) 2723.
- [66] C. Y. Wong, E. S. Swanson, and T. Barnes, Phys. Rev. C 62 (2000) 045201; Phys. Rev. C 65 (2002) 014903 [Erratum-*ibid.* C 66 (2002) 029901].
- [67] C. M. Ko, B. Zhang, X. N. Wang and X. F. Zhang, Phys. Lett. B 444 (1998) 237.
- [68] F. O. Duraes, H. Kim, S. H. Lee, F. S. Navarra, and M. Nielsen, Phys. Rev. C 68 (2003) 035208.
- [69] W. Cassing, L. A Kondratyuk, G. I. Lykasov, and M. V. Ryzanin, Phys. Lett. B 513 (2001) 1.
- [70] J. Geiss, C. Greiner, E. L. Bratkovskaya, W. Cassing, and U. Mosel, Phys. Lett. B 447 (1999) 31.
- [71] W. Cassing and E. L. Bratkovskaya, Nucl. Phys. A 623 (1997) 570.
- [72] W. Cassing and C. M. Ko, Phys. Lett. B 396 (1997) 39.
- [73] M. I. Gorenstein, A. P. Kostyuk, H. Stöcker, and W. Greiner, Phys. Lett. B 509 (2001) 277.
- [74] V. Friese, Nucl. Phys. A 774 (2006) 377.